Supporting Information

Steering Micromotors via Reprogrammable Optoelectronic Paths

Xi Chen[a,b,c,d], Xiaowen Chen [a], Mohamed Elsayed[b,d], Harrison Edwards[b,c], Jiayu Liu[a], Yixin Peng[a], Hepeng Zhang[e], Shuailong Zhang*[f,g], Wei Wang*[a], Aaron R. Wheeler*[b,c,d]*

[a] Sauvage Laboratory for Smart Materials, School of Materials Science and Engineering, Harbin Institute of Technology (Shenzhen), Shenzhen, 518055, China

[b] Institute of Biomedical Engineering, University of Toronto, Toronto, M5S 3E1, Canada.

[c] Department of Chemistry, University of Toronto, Toronto, M5S 3H6, Canada

[d] Donnelly Centre for Cellular and Biomolecular Research, University of Toronto, Toronto, M5S 3E1, Canada

[e] School of Physics and Astronomy and Institute of Natural Sciences, Shanghai Jiao Tong University, Shanghai, 200240, China

[f] School of Mechatronical Engineering, Beijing Institute of Technology, Beijing, 100081, China.

[g] Beijing Advanced Innovation Center for Intelligent Robots and Systems, Beijing Institute of Technology, Beijing, 100081, China.

Corresponding emails:

hepeng_zhang@sjtu.edu.cn, shuailong.zhang@bit.edu.cn, weiwangsz@hit.edu.cn, aaron.wheeler@utoronto.ca

1. SEM of Janus SiO_2-Pt Micromotor

Figure S1. Scanning electron microscope image of a SiO_2-Pt Janus microsphere.

2. Numerical simulations

To simulate the distributions of electric fields, a 3D finite element model was built in COMSOL Multiphysics (version 5.4) using Electric Current and Creeping Flow module. The model length (X-axis), width (Y-axis) and height (Z-axis) were set to be 500 μm, 500 μm, and 200 μm, respectively. The model included a 0.2 μm ITO and 1-μm-thick a-Si:H layer at the bottom and a 198.8-μm-thick liquid chamber.

The illuminated domain is a thin slab of 100×100×1 μm embedded at the bottom, and its electrical conductivity is set to be two orders of magnitude higher than the rest of the surface that is assumed to remain in darkness. The top surface of the entire solvable domain is grounded while the bottom surface (ITO layer) is set to 10V. Other surfaces are set to be insulating. See Fig. 3d for the configuration. Parameters were chosen following ref. 1.

In the Electric Current module, the boundary conditions were set to perfect electrical insulation at the sides. Top surface is grounded while the bottom surface is set to 10V to simulate the applied AC signal (frequency set to 100 kHz). The electric potential and electric field were calculated by solving the continuity equations:

$$\nabla \cdot \boldsymbol{J} = Q_{j,v} \qquad (Eqn.\ S1)$$

$$\boldsymbol{J} = \sigma \boldsymbol{E} + j\omega \boldsymbol{D} + \boldsymbol{J}_e \qquad (Eqn.\ S2)$$

$$\boldsymbol{E} = -\nabla V \qquad (Eqn.\ S3)$$

where $\boldsymbol{J}$ is the current density, $Q_{j,v}$ is the volumetric source of current, σ is the electrical conductivity, $\boldsymbol{E}$ is the electric field, ω is the angular frequency, $\boldsymbol{D}$ is the electric displacement, $\boldsymbol{J}_e$ is the externally generated current density, and V is the electrical potential.

Parameters used for this 3D model are listed in Table S1.

Table S1 COMSOL parameters for the optoelectronic system simulation

Parameter	Description	Value
σ_m	Conductivity of medium	5×10^{-5} S/m
ε_m	Electrical permittivity of medium	$80\varepsilon_0$
$\sigma_{silicon\text{-}light}$	Conductivity of amorphous silicon in the light	1×10^{-4} S/m
$\sigma_{silicon\text{-}dark}$	Conductivity of amorphous silicon in the dark	1×10^{-6} S/m
$\varepsilon_{silicon}$	Electrical permittivity of silicon	$11.7\varepsilon_0$

σ_{ITO}	Conductivity of ITO	5×10^5 S/m
ε_{ITO}	Electrical permittivity of ITO	4

Figure S2 below shows the simulation results of electrical potential and electric fields.

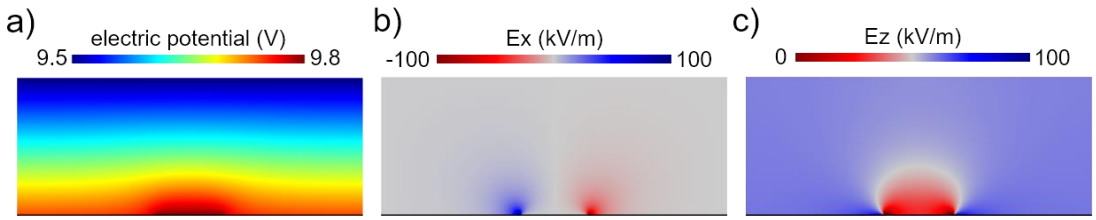

Figure S2. Additional results of the distributions of electrical potential and electric fields on the x-z cut plane. a): electrical potential. b): z (vertical) component of the electric field. c): x (horizontal or tangential) component of the electric field. Models are configurated according to Fig. S2, and the same as Fig. 3d and e in the main text.

3. Calculation of Re (K)

Re (K) is the real part of the Clausius–Mossotti factor. For calculation Re(K) of pure SiO_2, the expression is shown as follow:

$$K = \frac{\varepsilon_p^* - \varepsilon_m^*}{\varepsilon_p^* + 2\varepsilon_m^*} \qquad (Eqn.\ S4)$$

$$\varepsilon_p^* = \varepsilon_p - i\frac{\sigma_p}{\omega} \qquad (Eqn.\ S5)$$

$$\varepsilon_m^* = \varepsilon_m - i\frac{\sigma_m}{\omega} \qquad (Eqn.\ S6)$$

where ε_m and ε_p are the permittivity of the medium and the particle, and σ_m and σ_p are electrical conductivity of medium and particle. ω is the driving frequency of the electric field.

The σ_m of a 1:1 electrolyte of valence of z is:

$$\sigma_m = \sigma_m^+ + \sigma_m^- = \frac{z^2 e^2 N_A c_0}{k_B T}(D^+ + D^-) \qquad (Eqn.\ S7)$$

where + and – correspond to the cation and anion, respectively, and D is the ion diffusivity. c_0 is the ion concentration in the bulk, and N_A is the Avogadro number.

As preparing core-shell Pt-coated particles can be challenging, we have opted to use core-shell Ag-coated SiO_2 particles as an example to calculate the core-shell metal-coated SiO_2 particles. The expression for this calculation is shown below:

$$K = \frac{\varepsilon^*_{\text{core-shell}} - \varepsilon^*_{\text{m}}}{\varepsilon^*_{\text{core-shell}} + 2\varepsilon^*_{\text{m}}} \qquad (Eqn.\ S8)$$

$$\varepsilon^*_{core-shell} = \varepsilon^*_{Ag}\left[\gamma^3 + 2\left(\frac{\varepsilon^*_{SiO_2} - \varepsilon^*_{Ag}}{\varepsilon^*_{SiO_2} + 2\varepsilon^*_{Ag}}\right)\right] \Big/ \left[\gamma^3 - \left(\frac{\varepsilon^*_{SiO_2} - \varepsilon^*_{Ag}}{\varepsilon^*_{SiO_2} + 2\varepsilon^*_{Ag}}\right)\right] \qquad (Eqn.\ S9)$$

$$\gamma = \left(\frac{R}{r}\right)^3 \qquad (Eqn.S10)$$

$$\varepsilon^*_{SiO_2} = \varepsilon^*_p \qquad (Eqn.S11)$$

$$\varepsilon^*_{\text{Ag}} = \varepsilon_{\text{Ag}} - i\frac{\sigma_{\text{Ag}}}{\omega} \qquad (Eqn.S12)$$

where R and r are the outside and inner radius of Ag-coated SiO_2, ε_{Ag} is the permittivity of Ag, σ_{Ag} is the electric conductivity of Ag.

The values used in calculating Re(*K*) are listed in Table S2.

Table S2 Parameters for calculating Re(*K*)

Parameter	Description	Value
T	Temperature	293.15 K
ζ_p	Particle zeta potential	-0.05 V
ε_m	Electrical permittivity of water	$78.5\varepsilon_0$
ε_p	Electrical permittivity of SiO_2	$3.9\varepsilon_0$
ε_{Ag}	Electrical permittivity of Ag	1×10^9
D_+	Diffusivity of Na^+	1.33×10^{-9} $m^2\cdot s^{-1}$
D_-	Diffusivity of Cl^-	2.03×10^{-9} $m^2\cdot s^{-1}$
η	Dynamic viscosity of water at 293.15 K	1.0016×10^{-3} $Pa\cdot s^{-1}$
σ_p	Conductivity of SiO_2	1×10^{-10} $S\cdot m^{-1}$
σ_{Ag}	Conductivity of Ag	6.3×10^6 $S\cdot m^{-1}$

r	Radius of SiO_2	2.5×10^{-6} m
R	Radius of Ag-coated SiO_2	2.51×10^{-6} m
c_0	Ion concentration of bulk solution	1×10^{-4} mol·L^{-1}

Re(K) of Janus metal-SiO_2 microsphere can be calculated by averaging the Re(K) of pure SiO_2 microsphere and core-shell metal-coated SiO_2 microsphere.[2]

4. Explanation of using 0.1 mM NaCl liquid medium in our experiment

It is found that the ICEP self-propulsion micromotor at 100 kHz is strong at the 0.1 mM NaCl liquid medium, making it easy to control the movement of the micromotor in the OET system.

For the metallo-dielectric Janus particle, the self-propulsion speed is dependent on the electric field frequency.[3] At low frequency, Janus particle move with dielectric side forward due to ICEP. At low frequencies, the Janus particle moves with the dielectric side forward due to ICEP. However, as the frequency increases, the speed of the Janus particle slows down because the ions are unable to follow the rapid changes of the electric field, thereby failing to establish a fully charged electrical double layer (EDL). When the frequency reaches a crossover frequency, the Janus particle reverses its direction of movement.

In the OET system, the ICEP micromotor moves slowly at low ionic concentrations, likely because the driving frequency is close to the crossover frequency. As the charging frequency of the EDL scales with the square root of the ionic concentration, the crossover frequency increases with higher ionic concentrations. Therefore, increasing the ionic concentration to 0.1 mM enables the driving frequency of OET to be within the range that induces the ICEP effect, resulting in strong self-propulsion of the Janus particle. However, further increases in ionic concentration can weaken the ICEP speed due to screening of the electric field at high conductivity.[4] Therefore, we select the 0.1 mM NaCl liquid medium to perform our experiment.

4. Other supporting figures

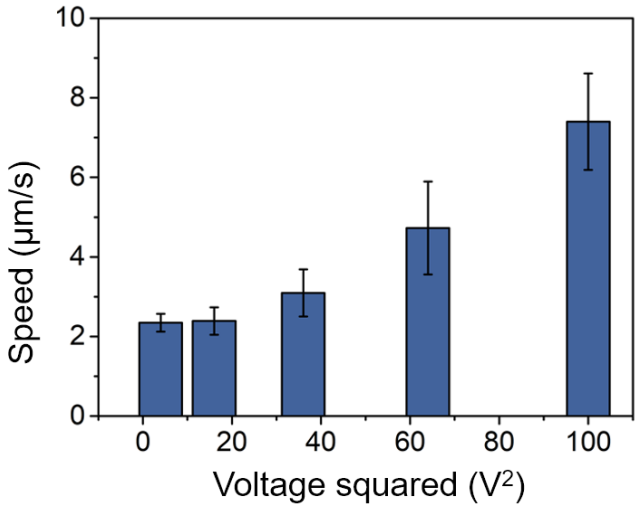

Figure S3. Speeds of SiO_2-Pt micromotors undergoing ICEP under different driving voltages in a typical sandwich electrode configuration (i.e., not an optoelectronic device)

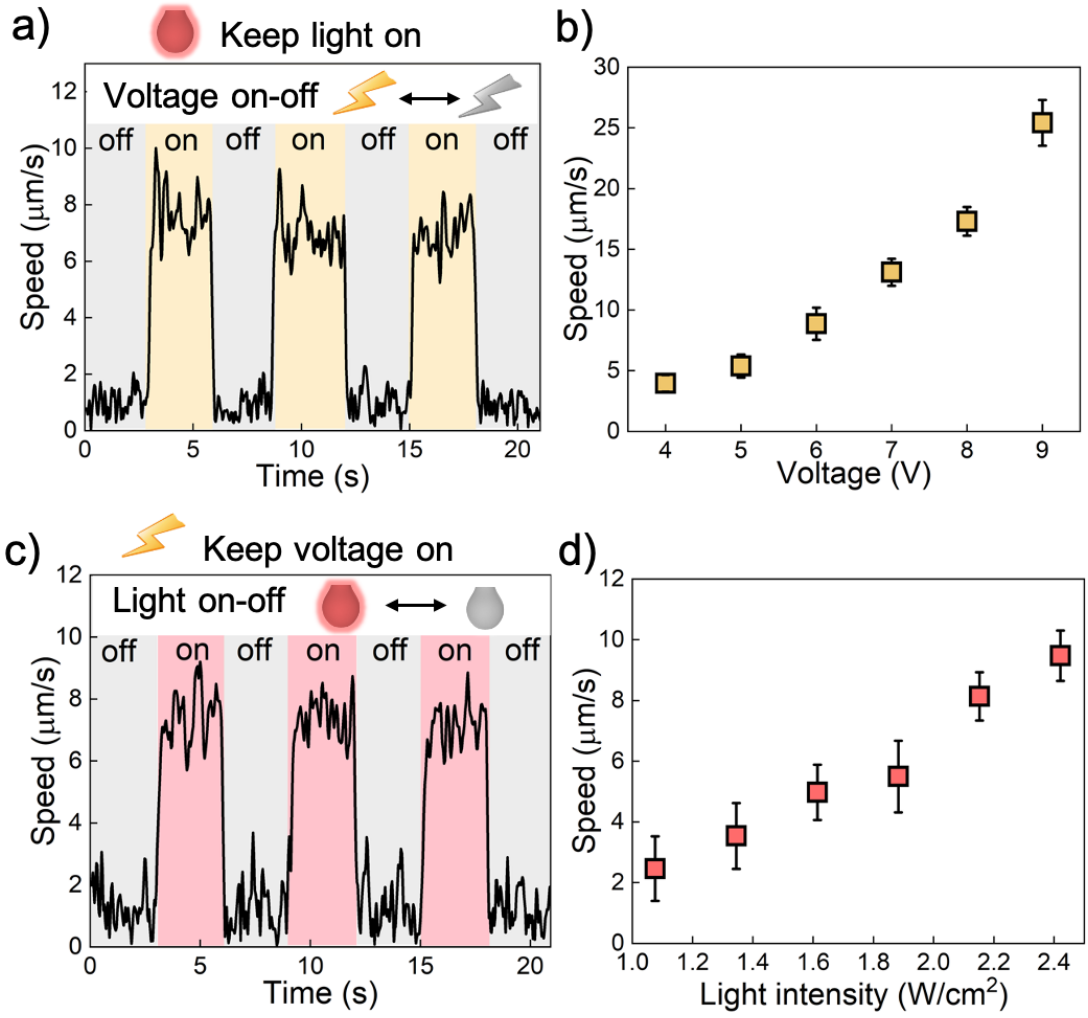

Figure S4. Speeds of SiO_2-Pt micromotors undergoing ICEP in an optoelectronic

device at different electric field conditions. (a, b): Motor speeds under constant illumination but varying voltages. (c, d): Motor speeds under constant voltages but varying light intensities.

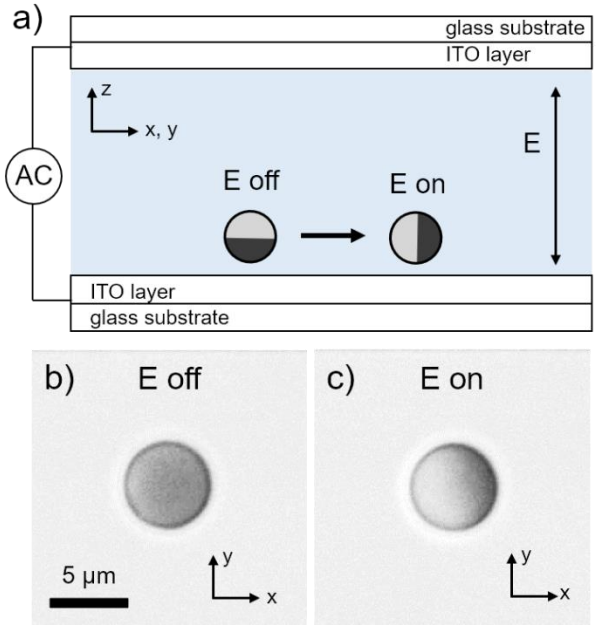

Figure S5. Alignment of metallo-dielectric Janus microspheres in an electric field. Here, polystyrene-gold Janus microspheres of 5 µm in diameter were suspended between two ITO electrodes separated by 200 µm. Upon turning on an AC electric field, their Janus interfaces quickly aligned with the field lines so they appeared half-black and half-white under an optical microscope.

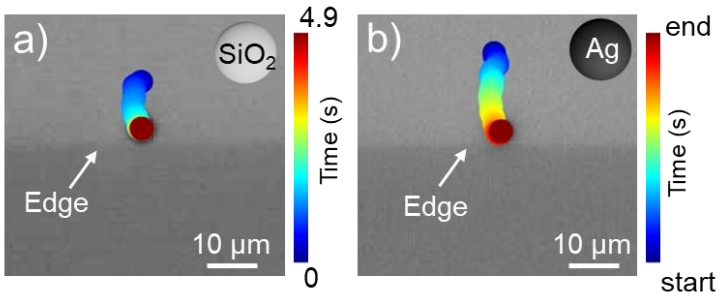

Figure S6. Both a SiO_2 microsphere (a) and a SiO_2 microsphere coated with an Ag shell (b) move to the light pattern's edge under an AC electric field of 100 kHz, exhibiting positive dielectrophoresis.

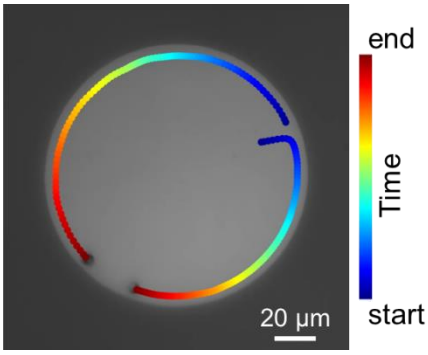

Figure S7. Two Janus SiO_2-Pt micromotors move clockwise or counterclockwise, respectively, in the circular light pattern under an AC electric field of 100 kHz.

5. Supporting Videos

All videos play at real time unless otherwise noted.

Video S1: SiO_2-Pt micromotors undergoing ICEP in and outside light patterns, corresponding to Figure 1c, d in the main text.

Video S2: SiO_2-Pt micromotors accumulating at and moving along light patterns, corresponding to Figure 2b, c in the main text.

Video S3: SiO_2-Pt micromotors steered by static light patterns, corresponding to Figure 4 in the main text.

Video S4: Spiral, helical and linear motion of a micromotor in dynamic light patterns, corresponding to Figure 5 in the main text.

Video S5: Collection and transport of five SiO_2-Pt micromotors by a dynamic light pattern, corresponding to Figure 6 in the main text.

Video S6: Au-Pt micromotors confined by light patterns, corresponding to Figure 7.

References

(1) Zhang, S.; Shakiba, N.; Chen, Y.; Zhang, Y.; Tian, P.; Singh, J.; Chamberlain, M. D.; Satkauskas, M.; Flood, A. G.; Kherani, N. P. Patterned optoelectronic tweezers: A new scheme for selecting, moving, and storing dielectric particles and cells. *Small* **2018,** *14* (45), 1803342.
(2) Zhang, L.; Zhu, Y. Dielectrophoresis of Janus particles under high frequency ac-electric fields. *Appl. Phys. Lett.* **2010,** *96* (14).
(3) Boymelgreen, A.; Yossifon, G.; Miloh, T. Propulsion of Active Colloids by Self-Induced Field Gradients. *Langmuir* **2016,** *32* (37), 9540-9547.
(4) Gangwal, S.; Cayre, O. J.; Bazant, M. Z.; Velev, O. D. Induced-Charge Electrophoresis of Metallodielectric Particles. *Phys. Rev. Lett.* **2008,** *100* (5), 058302.